JMEPEG (2009) 18:1102–1108
DOI: 10.1007/s11665-008-9336-z

1059-9495/$19.00

Effect of Alloying Elements on Tensile Properties, Microstructure, and Corrosion Resistance of Reinforcing Bar Steel

B.K. Panigrahi, S. Srikanth, and G. Sahoo

(Submitted July 31, 2008; in revised form November 21, 2008)

The effect of copper, phosphorus, and chromium present in a semikilled reinforcing bar steel produced by in-line quenching [thermomechanical treatment (TMT)] process on the tensile properties, microstructure, and corrosion resistance of steel in simulated chloride environment has been investigated. The results have been compared with that of a semikilled C-Mn reinforcing bar steel without these alloying elements produced by the same process route. Though the amount of phosphorus (0.11 wt.%) was higher than that specified by ASTM A 706 standard, the Cu-P-Cr steel exhibited a composite microstructure, and good balance of yield stress, tensile stress, elongation, and ultimate tensile to yield stress ratio. Two conventional test methods, namely, the salt fog, and potentiodynamic polarization tests, were used for the corrosion test. The rust formed on Cu-P-Cr steel was adherent, and was of multiple colors, while the corrosion products formed on the C-Mn steel were weakly adherent and relatively darker blue. Also, the free corrosion potential of the Cu-P-Cr steel was nobler, and the corrosion current was markedly lower than that of a C-Mn rebar. The Cu-P-Cr steel did not develop any pits/deep grooves on its surface even after the prolonged exposure to salt fog. The improved corrosion resistance of the Cu-P-Cr steel has been attributed to the presence of copper, phosphorus, and small amount of chromium in the dense, adherent rust layer on the surface of reinforcing steel bar. A schematic mechanism of charge transfer has been proposed to explain the improved corrosion resistance of the Cu-P-Cr alloyed TMT rebar.

Keywords alloy reinforcement bar, corrosion, microstructure, tensile properties, thermomechanical treatment

1. Introduction

High strength reinforcing steel bars (rebar) (yield stress: 420 MPa min), produced by in-line quenching thermomechanical treatment (TMT) process, are the backbone for general construction, and are used in combination with cement concrete for reinforced cement concrete (RCC) structures (Ref 1). The properties of these rebars are usually modified by alloying with suitable elements for use in specific areas such as seismic prone zones, and corrosive environments: coastal, marine, and industrial. When used in marine, and regions with high humidity content, the rebars should have good corrosion resistance properties. In seismic zones, the specific ultimate tensile to yield stress (UTS/YS) ratio should be maintained close to 1.25 as specified by ASTM A 706:2006 (Gr. 60).

The TMT process for rebars involves rolling billets in a continuous mill comprising roughing, intermediate, and finishing stands. The finish rolling temperature of billets is maintained relatively on higher side (about 1000 °C). After the finish rolling, the bar passes through an in-line quenching unit in which pressurized water is sprayed on the hot rebar to form a rim of martensite (M) on the surface of bar while the core still remains in austenite (γ) region. After emergence from the cooling unit, the heat transfer from the core of the bar to surface tempers the outer martensitic rim (T_m). Eventually, the core transforms to a two-phase ferrite (F)-pearlite (P) structure or a mixed structure depending upon the alloying elements present in the steel (Ref 2). The TMT process is schematically shown in Fig. 1.

Carbon-manganese steel rebars are subjected to corrosive attack in the RCC structure, particularly in marine environment when threshold chloride concentrations are exceeded especially at high temperature and humidity (Ref 3). The corrosion is aggravated by diffusion of chloride ions through micropores of concrete. The diffusion of chloride follows the second Fick's law (Ref 4):

$$\frac{\partial c_x}{\partial t} = D\frac{\partial^2 c_x}{\partial x^2} \quad \text{(Eq 1)}$$

Equation 1 can be solved for boundary conditions: $c = c_o$ at $t = 0$, $0 < x < \infty$, and $c = c_s$ at $x = 0$, $0 < t < \infty$ to yield

$$c_x = c_s(1 - \text{erf}\ x/2\sqrt{Dt}) \quad \text{(Eq 2)}$$

where c_s is the surface chloride concentration (%), c_x the proportion of chloride at a certain depth (%), D the chloride diffusion coefficient (m^2/s), x the depth of penetration (mm), t the time (s), and erf is the Gaussian error function.

When chloride reacts with steel substrate, the following reactions occur (Ref 5):

B.K. Panigrahi, S. Srikanth and **G. Sahoo**, Steel Authority of India Limited, Research and Development Center, Ranchi 834002, India. Contact e-mail: dr.bkpanigrahi1948@gmail.com.

$$Fe \rightarrow Fe^{2+} + 2e^{-} \quad \text{(Eq 3)}$$

$$Fe^{2+} + 2Cl^{-} \rightarrow 2[FeCl\ complex]^{+} \quad \text{(Eq 4)}$$

$$[FeCl\ complex]^{+} + 2OH^{-} \rightarrow Fe(OH)_2 + Cl^{-} \quad \text{(Eq 5)}$$

$$4Fe(OH)_2 + 2H_2O + O_2 \rightarrow 4Fe(OH)_3 \quad \text{(Eq 6)}$$

$$2Fe(OH)_3 \rightarrow Fe_2O_3 + 3H_2O \quad \text{(Eq 7)}$$

$$O_2 + 2H_2O + 4e^{-} \rightarrow 4OH^{-} \quad \text{(Eq 8)}$$

The chloride ions are not consumed by oxidation, and thereby contribute to corrosion as shown by Eq 4 and 5.

Cement contains calcium hydroxide which produces calcium carbonate (chalk) in the presence of carbon dioxide, and moisture in the environment (Ref 1, 6). The formation of carbonic acid in the cement micropores also lowers the pH of water in the pores of concrete close to 8 from 13.0 to 13.5, making the steel rebar vulnerable to corrosion. The depth of penetration of CO_2 is determined by the rate, which depends primarily upon the temperature, and the concentration of CO_2 at the surface of concrete. The depth of penetration (x) varies with the time (t), and follows a parabolic relationship (Ref 4):

$$x = k\sqrt{t} \quad \text{(Eq 9)}$$

where k is a constant dependent on the concrete thickness and ambient temperature.

Calcium carbonate also deposits in the pores, and with time the pH of pore water gets reduced to about 8 and may contain products of hydration, namely, silicates, aluminates; and the ferrite in steel becomes unstable, and corrodes. The corrosion products or rust being more voluminous exert pressure on the surrounding concrete and lead to localized spalling. The corrosive attack can be severe due to wind-borne chloride ions from sea that can penetrate through the micropores in concrete. The corrosion is aggravated by high humidity and temperature.

One of the practical methods available in mitigating corrosion without sacrificing tensile properties (Ref 7) is modification of alloy chemistry by addition of corrosion inhibiting alloying elements such as copper, phosphorus, chromium, molybdenum, and nickel in steel. In this article, the effect of these alloying elements on the tensile properties, microstructure, and corrosion resistance of a semikilled TMT reinforcing steel bar has been discussed.

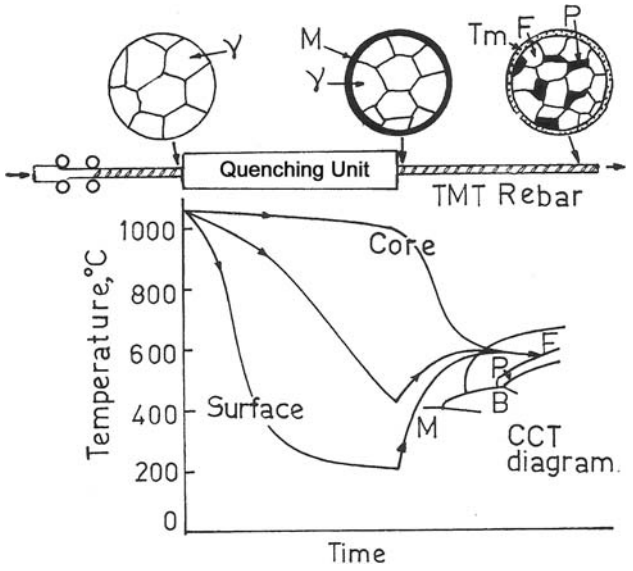

Fig. 1 Schematic of the TMT process for rebar

2. Materials and Procedure

Figure 2 shows the general view of a 32-mm-diameter TMT rebar with transverse ribs prior to its use in the reinforced structure. In this study, 70-mm-long cut pieces of a C-Mn TMT rebar conforming to ASTM A 706 (Gr. 60) along with a Cu-P-Cr TMT rebar of 32-mm diameter each were used. For optical microscopy, 15-mm-long pieces were cut from both the rebars, polished on the transverse section, and etched in 2% nital. The hardness of rim, transition zone, and core of alloy rebar was evaluated using a Vickers microhardness tester with a load of 0.49 N. Five indentations were made in each zone to calculate the average hardness for each zone.

Samples of C-Mn, and Cu-P-Cr alloyed TMT rebars 70 mm in length, were exposed in a salt fog chamber in duplicate as per ASTM B-117 for evaluating the corrosion behavior in chloride environment. A solution of NaCl (5%) was used to generate salt fog intermittently (20 min of spray time followed by 40 min of drying time) to simulate wetting, and drying cycles in the chamber. The rebar samples were removed from the chamber after 90 days (2160 h) and rinsed with water to remove any leftover salt deposits from the surface, and dried. The TMT rebar samples were subsequently cleaned free of corrosion products using Clarke's solution (ASTM G1:1981).

Potentiodynamic polarization scans were also performed to assess the corrosion behavior of rebars in 3.5% NaCl solution as per ASTM G 5. The tests were conducted using an EG&G PARC, Model 273A potentiostat, and a three electrode cell, wherein the rebar sample, saturated calomel, and graphite were used as working, reference, and auxiliary electrodes, respectively. The test was performed at a scan rate of 1 mV/s. Five samples were tested for each steel composition to ensure the reproducibility of results.

3. Results

3.1 Visual Examination

The surface of as-rolled TMT rebar (Fig. 2) did not show any pits or groves. However, the surface of the corroded rebars was irregular with corrosion products filling the valleys between the transverse ribs. The corrosion products (rust) were

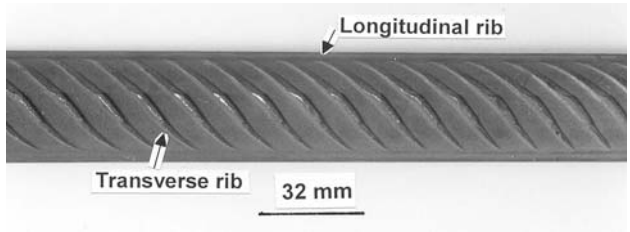

Fig. 2 General view of a 32-mm-diameter rebar

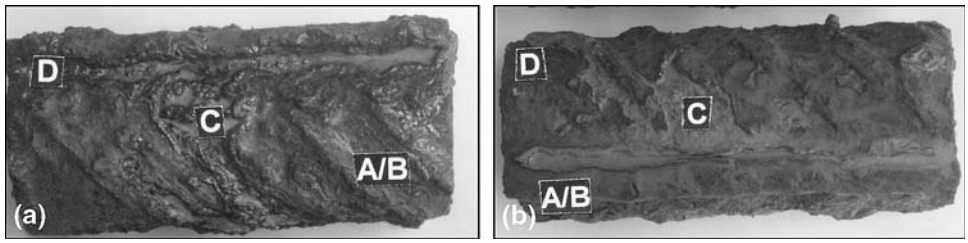

Fig. 3 Appearance of rust developed on (a) C-Mn rebar and (b) alloy rebar: (A) goethite, (B) akaganeite, (C) lepidocrocite, and (D) magnetite

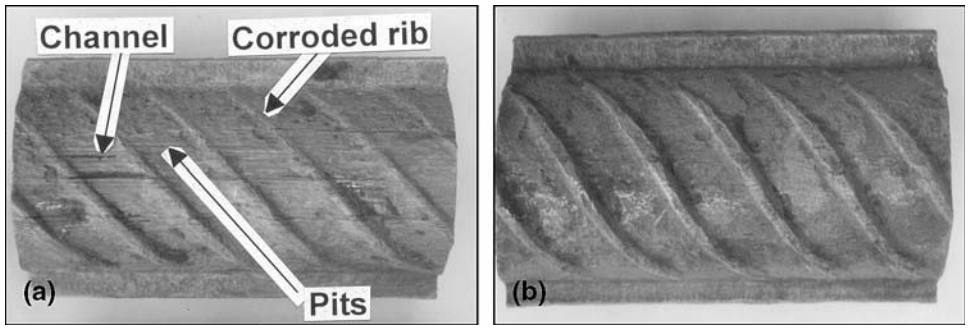

Fig. 4 Appearance of the surface of rebars after removal of corrosion product: (a) C-Mn rebar and (b) alloy rebar

Table 1 Chemical composition (wt.%) of experimental reinforcing steels along with as-specified composition in the standard

Steel	C	Mn	Si	S	P	Cu	Cr	N, ppm
C-Mn	0.19	1.14	0.01	0.020	0.018	Trace	Trace	63
Cu-P-Cr	0.14	0.75	0.04	0.028	0.107	0.33	0.13	81
ASTM A 706 Gr. 60	0.30 max	1.50 max	0.50 max	0.04 max	0.035 max	…	…	…

of varying color and hue (Fig. 3). The dark brown corrosion products are presumed to be α-FeOOH (goethite) (A) and β-FeOOH (akaganeite) (B); the orange colored rust is γ-FeOOH (lepidocrocite) (C); and the blackish regions are Fe_3O_4 (magnetite) (D) (Ref 8). The comparative appearance of the surface of rebars after the removal of rust is shown in Fig. 4. The surface of C-Mn TMT rebar showed several pits and a few longitudinal channels up to 1.5 mm deep running across the helical transverse ribs (Fig. 4a), whereas the surface of Cu-P-Cr alloyed rebar was relatively free from pits and channels (Fig. 4b).

3.2 Chemical Composition

As shown in Table 1, the C-Mn steel is a medium carbon steel with carbon, and manganese higher than alloy steel, and conforms to ASTM A 706 standard. The alloyed steel had copper, phosphorus, and chromium. The content of phosphorus in Cu-P-Cr alloyed rebar was higher than that stipulated by the standard.

3.3 Tensile Properties

Table 2 presents the tensile properties of the investigated rebars. It was observed that the yield stress, UTS, and percent elongation of both the steels conform to ASTM A 706 standard. However, UTS/YS ratio of C-Mn steel was lower than the specified minimum value of 1.25 as per this standard.

Table 2 Tensile properties of experimental reinforcing steels along with properties as specified in the standard for 32-mm-diameter bar

Steel	Yield stress (YS), MPa	Ultimate tensile stress (UTS), MPa	UTS/YS	Total elongation, %
C-Mn	519	636	1.22	21
Cu-P-Cr	512	640	1.25	20
ASTM A 706 Gr. 60	420-540	550 min	1.25 min	12 min
Bar diameter: 32 mm				

3.4 Macrostructure

The macrostructure of the as-rolled Cu-P-Cr alloyed steel rebar (b) on the transverse section is shown in Fig. 5. The

structure can be delineated into three distinctly separate regions. The darker region corresponds to tempered martensite rim, and is followed by an intermediate bainitic transition zone, and a ferrite-pearlite core. Similar microstructures were observed for C-Mn TMT rebar.

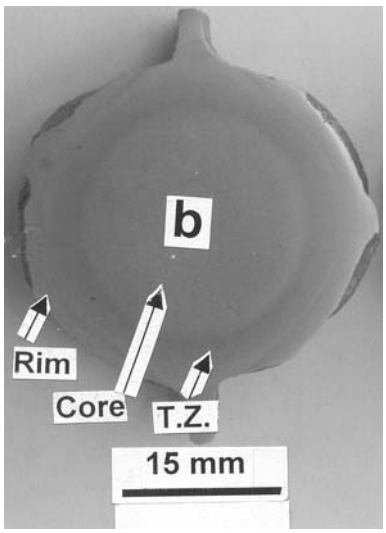

Fig. 5 Macrostructure of alloy rebar (b) in as hot rolled condition

3.5 Microstructure and Hardness

Figure 6 shows the composite microstructure of TMT rebars comprising rim, transition zone, and core. The rim (Fig. 6b, top) of Cu-P-Cr alloyed TMT rebar showed tempered martensite (Hardness 287 VHN). The transition zone (Fig. 6b, mid) adjacent to the rim revealed bainitic structure (Hardness 258 VHN). The core (Fig. 6b, bottom) showed a mixed structure (Hardness 229 VHN) comprising non-polygonal ferrite (NPF), polygonal ferrite (PF), Fe_3C (cementite), and bainite (B). In comparison, the rim (Fig. 6a, top) of C-Mn rebar showed a tempered martensite structure (Hardness 286 VHN). The transition zone (Fig. 6a, mid) was predominantly bainitic (Hardness 216 VHN), and the core (Fig. 6a, bottom) showed a polygonal ferrite-pearlite structure (Hardness 185 VHN).

3.6 Salt Spray Test

Table 3 shows the corrosion rate of reinforcing steels after 90 days exposure in salt fog chamber. The corrosion rate of the

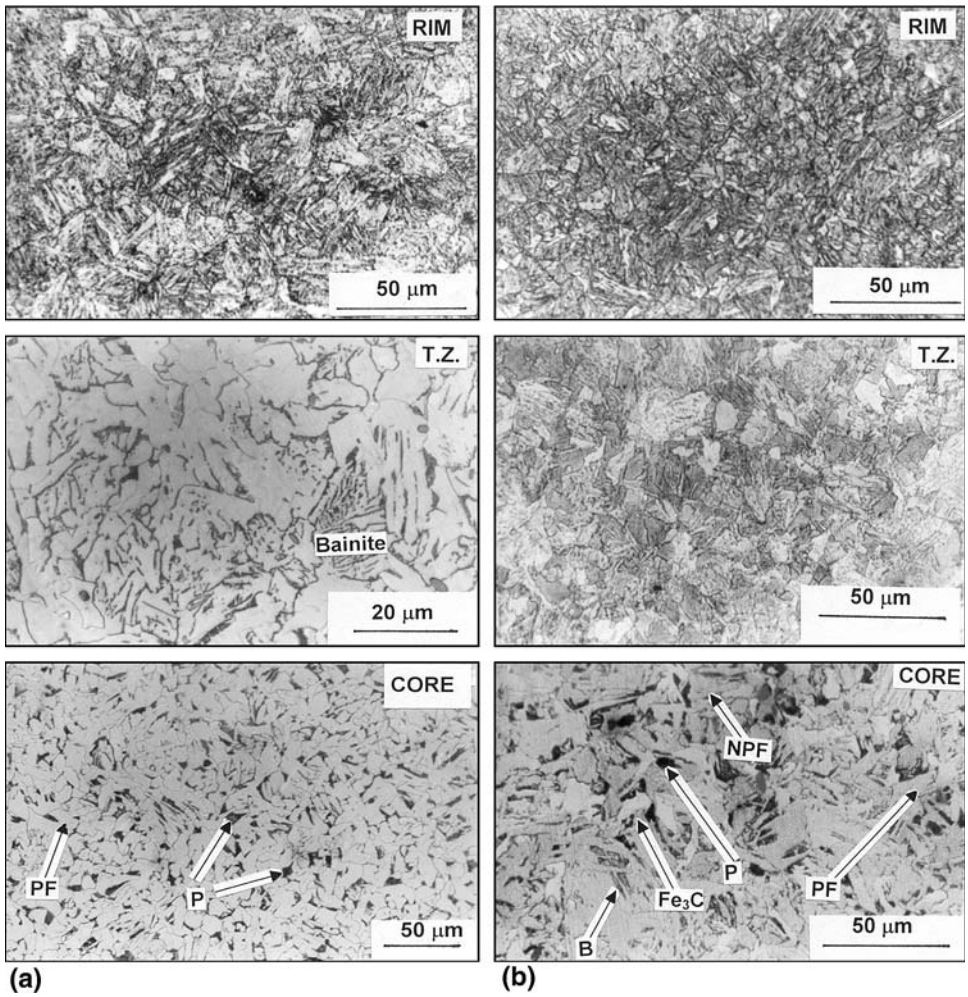

Fig. 6 Microstructure of (a) C-Mn rebar and (b) alloy rebar: PF, polygonal ferrite; NPF, non-polygonal ferrite; P, pearlite; B, bainite; Fe_3C, cementite

rebars was calculated using the following equation after exposure in salt spray as per ASTM G 1:

$$\text{Corrosion rate (mpy)} = \frac{kW}{Atd}$$

where $k = 3.45 \times 10^6$, W is the weight loss (g), d the density of steel (g/cm^3), A the area (cm^2), and t is the exposure time (h).

It can be inferred from the table that the ratio of corrosion rates of C-Mn, and Cu-P-Cr TMT rebars, i.e. the corrosion resistance index (CRI) of Cu-P-Cr rebar, is 1.74.

3.7 Potentiodynamic Test

The potentiodynamic polarization behavior of the Cu-P-Cr alloyed and C-Mn TMT rebars in 3.5% NaCl solution is depicted in Fig. 7. The corresponding electrochemical parameters are shown in Table 4. While the free corrosion potential and corrosion current density of Cu-P-Cr rebar were −410 mV and 93.80 μA/cm^2, respectively, the C-Mn rebar exhibited more active corrosion potential (−560 mV) and higher current density (169.2 μA/cm^2). The corrosion rates of Cu-P-Cr TMT rebar and C-Mn TMT rebar were found to be 2.16 and 3.84 mpy, respectively. This translates into a CRI (ratio of the corrosion rate of C-Mn and Cu-P-Cr rebars) of 1.77 for the Cu-P-Cr rebar.

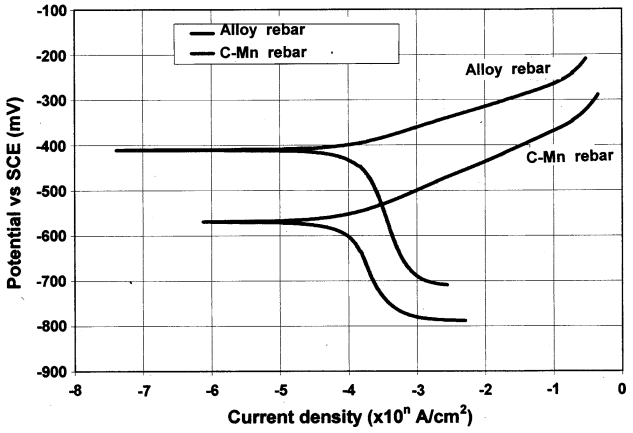

Fig. 7 Potentiodynamic polarization behavior of C-Mn rebar and alloy rebar in 3.5% aqueous NaCl

Table 3 Corrosion rates of reinforcing steels after 90 days exposure to 5% salt fog

Steel	Area, cm^2	Initial weight, g	Final weight, g	Corrosion rate, mpy
C-Mn	68.2	431.0	419.6	34.0
Cu-P-Cr	68.8	435.8	429.2	19.5

Table 4 Electrochemical parameters and corrosion rates of reinforcing steels obtained from potentiodynamic polarization test in 3.5% NaCl solution

Steel	Free corrosion potential (mV versus SCE)	Corrosion current, μA	Corrosion rate, mpy
C-Mn	−560.2	169.2	3.849
Cu-P-Cr	−410.9	93.8	2.162

4. Discussion

The build-up of rust or iron oxide proceeds by anodic and cathodic reactions on iron and steel substrate that involves transfer of charge. Though there are 16 types of known iron oxides (Ref 8), only goehite (α-FeOOH), akaganeite (β-FeOOH), lepidocrocite (γ-FeOOH), and magnetite (Fe_3O_4) were found in the corrosion products of the investigated reinforcing steels. α-FeOOH or goethite structure consists of hexagonal close packed array of anions (O^{2-} and OH^-) stacked along [010] direction with Fe^{3+} ions located in half of the available interstices. γ-FeOOH or lepidocrocite structure consists of arrays of cubic close packed anions arranged along [150] direction with Fe^{3+} ions in octahedral interstices. In β-FeOOH or akaganeite structure, anions are arranged in a body centered cubic array with Fe^{3+} ions in octahedral interstices. In Fe_3O_4 or magnetite, 32 oxygen ions are arranged in [111] direction of face-centered cubic unit cell with Fe^{3+} ions occupying both tetrahedral and octahedral sites. In these oxides, cations other than Fe can also occupy the vacant sites of the arrays of anions (oxygen) subject to the condition involving similarity of the ionic radii, and the valency of cations.

When alloying elements are used, they increase the driving electromotive force required for corrosion to occur due to poor electron transfer behavior of the barrier at metal/environment interface. Phosphorus, chromium, and copper are alloying elements in the present alloyed TMT rebar. Sulfur is an impurity element (Ref 9). Nitrogen is also an impurity but due to its relatively low concentration (81 ppm) it is not detrimental to the rebar steel. The alloy design ensured low carbon and sulfur. Carbon is detrimental since it forms pearlite in as-rolled steel, making the steel vulnerable to micro-galvanic corrosion. Carbon also reduces the breakdown potential (Ref 10) (Table 5) of passive film on steel. A negative breakdown potential is liable to favor diffusion of chloride ions to the steel substrate.

In a TMT rebar, tempered martensite formed from higher carbon steel is likely to corrode faster than that of low carbon steel tempered martensite in chloride environment. This is because the Ms temperature of steel with lower carbon is at a

Table 5 Effect of alloying elements on breakdown potentials (BDP) of steel in chloride solution at ambient temperature (Ref 10)

Elements	Shift in BDP to more positive or negative potential values
C	(−)
Si	(+)
Cr	(+)
Mo	(+) at ambient temperature (−) at 0 °C
Ni	(+)
Nb	(−)
V	(+)
Ti	(−)
P	(+) presumed for Cu-P-Cr alloyed TMT rebar

higher level, and the driving force necessary for the transformation to martensite in low carbon steel is smaller. Consequently, the density of mobile dislocations present in low carbon tempered martensite will be smaller (Ref 11). Manganese is a substitutional solid solution strengthener, increases hardenability, and forms MnS inclusions. Elongated MnS inclusions are detrimental particularly when they lie close to the surface. Higher amount of manganese in alloy rebar could favor bainitic transformation in the core affecting the ductility of rebar.

Copper has a beneficial effect in increasing the corrosion resistance of steel due to the formation of a very thin oxide film on the steel surface (Ref 12, 13). Phosphorus has been used in alloy rebar in relatively higher amount (0.11 wt.%) similar to a weathering steel (P0.08-0.15 wt.%). The solubility of phosphorus in α-iron at room temperature is low (Ref 14). In a phosphorus bearing steel with 0.11 wt.% phosphorus, the atoms of phosphorus are in substitutional solid solution of α-iron, causing the strengthening effect of ferrite in the TMT rebar. Phosphorus also increases the hardenability of steel. Phosphorus is generally perceived as an embrittling element in steel due to its segregation tendency to grain boundaries. The segregation of phosphorus lowers the fracture toughness of steel. In structural steel, interstitial carbon diffuses to the ferrite grain boundaries in preference to phosphorus since the Gibb's free energy for grain boundary segregation of carbon in ferrite is lower (−72 kJ/mol) than Gibbs free energy for grain boundary segregation of phosphorus in ferrite (−49 kJ/mol), and the grain boundary embrittlement tendency in phosphorus steel is minimized (Ref 15). Though the highest segregation occurs at 550-600 °C, special measures were taken to eliminate this by control of rolling and in-line quenching parameters of TMT rebar. Presence of phosphorus in steel increases its corrosion resistance in coastal region (Ref 16) and is very effective when added with small amount of copper (Table 6). It makes the surface rust layer impervious, dense, and adherent compared to the rust layer on C-Mn steel which is relatively, porous, loose, and often ridden with fissures. It has been observed in weathering steel that the rust layer has an amorphous structure (Ref 17), with the presence of Cu, P, Ni, and Cr in it (Ref 12). This layer is also non-porous and adherent.

Quantum mechanical calculations by Briant and Messmer (Ref 18) have shown that phosphorus is more electronegative with respect to iron and draws charge off the host metal on to itself as shown schematically in Fig. 8. According to the electronegativity scale of Pauling (Ref 19), chromium is more electronegative with respect to iron, as a result of which chromium atoms draw charge from iron (Fig. 8). The implication of this is that the availability of charge (electrons in 3d orbital of iron) for anodic reaction is greatly reduced, and corrosion is hindered.

As shown in Fig. 4, the Cu-P-Cr alloyed rebar was free of pits after the removal from the salt spray chamber which could be due to the densely adherent rust formed on the surface. Copper, chromium, and possibly phosphorus have increased the breakdown potential of the passive film (Ref 10). This is advantageous in the formation of a homogenous rust layer of densely packed α-FeOOH (goethite), with alloying elements (cations) in vacant sites (Ref 8) of the interstices of oxygen frame work. The layer being poor conductor of electrons could hinder the diffusion of chloride ions to steel substrate retarding the corrosion. The β-FeOOH (akaganeite) and γ-FeOOH (lepidocrocite) have possibly alloying elements in vacant sites stabilizing it, and preventing ingress of ions to steel substrate. The rust layer of Cu-P-Cr alloyed rebar was also free from cracks, and well adherent. In contrast, the rust formed on C-Mn steel was composed of coarser particles (Ref 20) and was ridden with fissures. Enrichment of alloying elements in the rust is likely to scatter electrons and restrict the free flow of electrons across the surface film, diminishing the tendency of rusting.

A minimum content of copper (about 0.20 wt.%) is desired to obtain satisfactory corrosion resistance (Ref 17). Phosphorus content of the alloy rebar was 0.11 wt.%. Below 0.08 wt.% phosphorus, solid solution strengthening and corrosion retarding effect due to phosphorus are insignificant, and above 0.15 wt.% phosphorus, embrittlement may arise in medium carbon steel depending upon the alloying elements present in the steel, particularly chromium and manganese (Ref 18). Due to electronegativity effect, phosphorus will draw charge from chromium and manganese, and thereby the total charge on phosphorus will increase. As a result, lesser charge is available

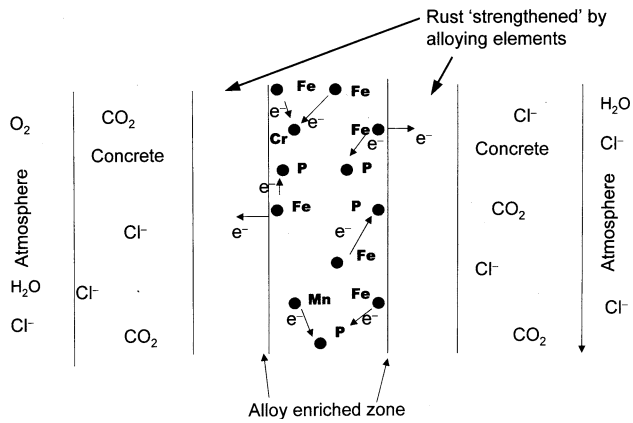

Fig. 8 Schematic charge transfer mechanism in the Cu-P-Cr alloyed reinforcing bar

Table 6 Effect of alloying elements on the corrosion resistance of unalloyed steel in seawater (Ref 16)

Element	Decreasing effect in corrosion rate	Remarks
P	Effective in seawater and splash water, effect is intensified by copper	Significant influence
Cu	Very effective in seawater, splash water zone, and in sea atmosphere	…
Cr	Very effective, effect is intensified by copper	…
Al	Significant influence particularly in combination with copper	…
Ni, Si, Mo, Co	Not as effective in seawater as in aggressive atmosphere	Low influence
C	Accelerates corrosion	Adverse influence
Mn	Slight corrosion acceleration	…
S	No adverse influence in copper alloyed steel	…

to participate in the metal-metal bonds, and the bonding becomes weak leading to embrittlement. Hence, chromium and manganese are kept at low level in the presence of phosphorus. Lower amount of manganese should also facilitate the availability of free interstitial carbon for displacing phosphorous from ferrite grain boundaries for improved mechanical properties (Ref 15). The present Cu-P-Cr alloyed steel was found to possess a good balance of strength, UTS/YS ratio, elongation, and corrosion resistance.

5. Conclusions

The results of investigation of a Cu-P-Cr alloyed and a C-Mn steel TMT rebar can be summarized as follows.

1. Both the rebars exhibited composite macro and microstructures comprising tempered martensitic rim followed by an intermediate bainitic region. However, the core of Cu-P-Cr alloyed rebar revealed mixed ferrite-pearlite structure with some bainite in contrast to the predominantly ferrite-pearlite core of C-Mn rebar.
2. The tensile properties of both reinforcing steels conformed to ASTM A 706 specifications. The UTS/YS ratio of Cu-P-Cr alloyed rebar conformed to the specified value (1.25) as per the standard.
3. The corrosion resistance index of Cu-P-Cr alloyed reinforcing steel was 1.7 with respect to C-Mn steel as determined by both salt fog and potentiodynamic polarization tests. The rust formed on the Cu-P-Cr rebar was found to be adherent and of multiple colors.
4. A schematic charge transfer mechanism has been proposed to explain the role of alloying elements like Cu, Cr, and P on the formation of protective rust layer on alloyed TMT rebar.
5. The Cu-P-Cr alloyed reinforcing steel exhibited a good balance of strength, UTS/YS ratio, ductility, and corrosion resistance.

Acknowledgments

The authors thank the management of Steel Authority of India Limited, Bhilai Steel Plant, and R & D Center for Iron and Steel, Ranchi, India, for support. The authors also express their gratitude to Mr. Dhritiman Panigrahi, undergraduate student of Mechanical Engineering at Manipal Academy of Higher Education, Manipal, Karnataka, India, for preparation of drawings, and Mr. Sabyasachi Mahapatra, Lecturer in Physics, St. Pauls Cathedral Mission College, Kolkata, India, for discussion.

References

1. J.E. Slater, Corrosion of Structures, Corrosion: Environments and Industries, *ASM Handbook*, Vol 13C, American Society of Metals, OH, 2006, p 1054
2. B.K. Panigrahi and S.K. Jain, Impact Toughness of High Strength Low Alloy TMT Reinforcement Rebar, *Bull. Mater. Sci.*, 2002, **25**, p 319–324
3. C.A. Apostolopoulos and D. Michalopoulos, Effect of Corrosion on Mass Loss, and High and Low Cycle Fatigue of Reinforcing Steel, *J. Mater. Eng. Perform.*, 2006, **15**, p 742–749
4. C. Andrade and C. Alonso, Progress on Design and Residual Life Calculation with Regard to Rebar Corrosion of Reinforced Concrete, *Techniques to Assess the Corrosion Activity of Steel Reinforced Concrete Structures*, ASTM STP 1276, N.S. Berke, E. Escalante, C.K. Nmai, and D. Whiting, Eds. (Philadelphia), ASTM International, 1996, p 23–40
5. J. Balma, D. Darwin, J.P. Browning, and C.E. Locke, Evaluation of Corrosion Resistance of Microalloyed Reinforcing Steel, *Standard Engineering and Engineering Materials*, SM Report No. 71, University of Kansas Center for Research Inc., Lawrence, KS, December, 2002
6. V. Kumar, Protection of Steel Reinforcement Cocrete—A Review, *Corros. Rev.*, 1998, **16**(4), p 317–358
7. A.B. Yur'ev, Y.F. Ivanov, V.E. Gromov, and E.V. Kozlov, Structural–Phase State of Thermostrengthened Large Diameter Reinforcement, *Steel Transl.*, 2004, **34**(6), p 69–72
8. R.M. Cornell and U. Schwertmann, *The Iron Oxides*, 2nd ed., Wiley-VCH, Weinheim, 2003
9. B.K. Panigrahi, S. Srikanth, and J. Singh, Corrosion Failure of Steel in Sugar Industry—A Case Study, *J. Fail. Anal. Prev.*, 2007, **7**, p 187–191
10. S. Szklarska-Smialowska, The Pitting of Iron-Chromium-Nickel Alloys, *Localised Corrosion*, NACE, Houston, 1981, p 312–341
11. S. Morooka, Y. Tomota, and T. Kamiyama, Heterogenous Deformation Behavior Studied by In-Situ Neutron Diffraction During Tensile Deformation for Ferrite, Martensite, and Pearlite Steels, *ISIJ Int.*, 2008, **48**(4), p 525–530
12. M. Yamashita, H. Nagano, T. Misawa, and E. Townsend, Structure of Protective Rust Layers Formed on Weathering Steels by Long Term Exposures in the Industrial Atmosphere of Japan and North America, *Iron Steel Inst. Jpn. Int.*, 1998, **38**, p 285–290
13. K. Schwabe and W.D. Arnold, Behavior of Low Alloyed Steel, *Proc. 5th Intl. Congress on Metallic Corrosion* (Houston), NACE, 1971, p 760–763
14. J. Pilling, N. Ridley, and D.J. Gooch, The Effect of Phosphorus on Creep in 2.5% Cr-1% Mo Steels, *Acta Metall.*, 1982, **30**, p 1587–1595
15. H.J. Grabke, Effects of Impurities in Steels on Mechanical Properties and Corrosion Behavior, *Steel Res.*, 1987, **58**, p 477–482
16. *DECHEMA Corrosion Handbook*, Vol 11, G. Kreyser and R. Eckermann, Eds., VCH Publishers, New York, 1992, p 182
17. H. Okida, S. Sekino, Y. Hosoi, and T. Murata, Copper Containing Structural Steels, in *Copper in Iron and Steel*, I. LeMay and I.M. Shetky, Eds., Wiley, New York, 1982, p 83–93
18. C.L. Briant and R.P. Messmer, An Electronic Model for the Effect of Alloying Elements on the Phosphorus Induced Grain Boundary Embrittlement of the Steel, *Acta Metall.*, 1982, **30**, p 1811–1818
19. L. Pauling, *The Nature of the Chemical Bond*, 3rd ed., Cornell University Press, Ithaca, NY, 1960, p 93 ()
20. J. Davalos, J.F. Marco, M. Garcia, and J.R. Gancedo, The Corrosion Products of Weathering Steel and Pure Iron in Simulated Wet-Dry Cycles, *Hyper Interact.*, 1991, **66**, p 63–70